Non-dimensional analysis of experimental pressure drop and energy dissipation measurements in Oscillatory Baffled Reactors

J. Muñoz-Cámara, J.P. Solano, J. Pérez-García

Dep. Ing. Térmica y de Fluidos, Universidad Politécnica de Cartagena, Campus Muralla del Mar, 30202 Cartagena, Spain

HIGHLIGHTS

- The experimental study covers two baffle types, different viscosities and amplitudes.
- The oscillating pressure drop is analyzed by using a statistical fitting and the FFT.
- The conventional models are found to be valid only for $Re_{osc} > 150$.
- An adapted definition of the Power number provides consistent dimensionless results.
- A new experimental correlation is proposed for the Power number.

ARTICLE INFO

ABSTRACT

An experimental study is performed to characterize the pressure drop and the power consumption in Oscillatory Baffled Reactors, using dimensionless numbers: the oscillatory Fanning friction factor (f_{osc}) and the Power number (Po), respectively. Two baffle geometries (one-orifice and three orifices) are tested, for different fluids and oscillating amplitudes. The range of oscillatory Reynolds numbers (Re_{osc}) tested is 10–1000. Data reduction based on the statistical fitting and the FFT of the pressure drop and velocity signals is introduced to assess the maximum pressure drop and the phase lag between both signals. The new set of experimental data proves the limitations of the conventional models available in the open literature. f_{osc} and Po provide consistent dimensionless results for the different working fluids tested and their trends are clearly related to different flow behaviours: laminar or chaotic flow. Correlations for f_{osc} and Po as a function of Re_{osc} and dimensionless amplitude are obtained.

© 2022 Elsevier Ltd. All rights reserved.

1. Introduction

Oscillatory Baffled Reactors (OBR) have been a focus of interest during the last decades due to their effective mixing properties and overall adequacy for process intensification purposes. Some examples of chemical processes where they have been used are ozonification (Graca et al., 2020), crystallization (Onyemelukwe et al., 2020) or transesterification (Eze and Harvey, 2018). These devices are based on the superposition of an oscillatory flow onto a low net flow. Thus, there are two units requiring power: the main pump and the oscillator.

The quantification of the power consumption in OBRs has been a focus of attention for many researchers, due to its relevance to a correct sizing of the oscillatory flow system. In addition, the power consumption is necessary to compare the performance of the OBRs to different devices as stirred tanks (Liu et al., 2019). However, the

number of experimental studies related to power consumption is still scant as McDonough et al. (2015) highlighted.

The studies of the last decades can be divided in those focused on Oscillatory Baffled Columns (OBC), which served as a base for future studies on OBRs, and those focused on models for the energy dissipation in conventional OBRs.

The precedent works on energy dissipation in oscillatory flow devices were accomplished in 1955 by Jealous and Johnson (1955), who studied the power consumption in an extraction column under oscillatory flow conditions. The authors developed a quasi-steady predictive model, assuming that the frictional pressure drop at each instant is equal to the pressure drop in a steady flow with the same instantaneous flow velocity. The system was considered as a series of individual baffles, using the conventional discharge coefficient to model the pressure drop in each baffle.

Baird and Garstang (1967) studied the power consumption in an oscillating column with different baffle configurations. The results for different frequencies were compared with those

Nomenclature

A	cross-sectional area, (m^2)
d	orifice diameter (m)
D	tube inner diameter (m)
f	oscillation frequency (Hz)
l	cell length (m)
l_m	mixing length (m)
L_p	length between pressure ports (m)
n_o	number of orifices
n_b	number of baffles
S	open cross-sectional area
t	time (s)
T	oscillation period (s)
u	instantaneous mean flow velocity (m/s)
U_n	net mean flow velocity (m/s)
V	cell volume (m^3)
W	Average power dissipation over one cycle (W)
x	instantaneous piston position (m)
x_0	oscillation amplitude, center to peak (m)

Greek symbols

Δp	pressure drop (Pa)
Δp_{max}	maximum oscillatory pressure drop (Pa)
δ	pressure drop-velocity phase lag (rad)
ε_v	power density (W/m^3)
μ	dynamic viscosity (kg/(m·s))
ρ	fluid density (kg/m^3)
ω	angular frequency (rad/s)

Subscripts

ee	eddy enhancement model
osc	oscillatory flow
qs	quasi steady model

Dimensionless groups

C_0	discharge or orifice coefficient,	$\sqrt{\frac{\rho U_n^2}{2\Delta p}\left(1/S^2 - 1\right)}$
Re_n	net Reynolds number, $\rho U_n D/\mu$	
Re_{osc}	oscillatory Reynolds number, $\rho(2\pi f x_0)D/\mu$	
f_n	net Fanning friction factor, $\frac{\Delta p}{2\rho U_n^2}\frac{D}{L_p}$	
f_{osc}	oscillatory Fanning friction factor, $\frac{\Delta p_{max}}{2\rho(2\pi f x_0)^2}\frac{D}{L_p}$	
St	Strouhal number, $D/(4\pi x_0)$	
Po	Power number, $Po = \frac{\overline{W}_{osc}}{n_b \rho (2\pi f x_0)^3 D^2}$	

deducted using the quasi-steady model, obtaining deviations less than ± 10 % for the configuration with only one baffle, and deviations of a 30 % for the whole range tested for the baffle configuration in series.

Hafez and Baird (1978) studied the energy dissipation in an OBC with Karr type baffles. The quasi-steady model performed properly for the tests with high amplitudes and low frequencies, but underpredicted the power density at low amplitudes and high frequencies. The authors provided some possible causes of these discrepancies: the phase lag of the frictional pressure drop and/or the variation of the discharge coefficient. The authors referred to Daily et al. (1955): "it appears that unsteadiness produces an internal flow structure that is no longer comparable to any steady-state condition". Finally, the experimental results of power consumption, $\overline{W}_{osc}$, were fitted to a correlation using a dimensionless form for the power consumption: $(\overline{W}_{osc}/\overline{W}_{qs} - 1)$, where $\overline{W}_{qs}$ is the power consumption predicted by the quasi-steady model.

With the development of oscillatory baffled reactors (OBRs), the need for characterising the power consumption in these continuous flow devices led to the development of new models.

Mackay et al. (1991) introduced the power density concept, as the power consumption per volume unit, which is still widely used to characterise the energy dissipation in OBRs. The authors developed an expression for the average power consumption assuming that both the fluid velocity and the pressure drop are perfectly sinusoidal.

$$\overline{\varepsilon}_v = \frac{\overline{W}_{osc}}{V} = \frac{\overline{W}_{osc}}{n_b l A} \tag{1}$$

$$\overline{\varepsilon}_v = \frac{\Delta p_{max}\omega x_0 \cos(\delta)}{2 n_b l} \tag{2}$$

These authors performed numerical simulations, showing, for one-orifice baffles and $St = 1$, an increasing trend for the pressure drop-velocity phase lag, δ, which is almost null at $Re_{osc} = 0.1$ and reaches a value $\delta \approx 80°$ for $Re_{osc} = 100$. Above this value, the flow becomes more complex and the model does not fit the experimental flow patterns. Above $Re_{osc} = 200$, the phase lag decreases up to a value

of 0° at higher oscillatory Reynolds numbers, $Re_{osc} \approx 2000$. The authors suggested that the maximum phase lag coincides with the onset of the flow asymmetry.

Mackley and Stonestreet (1995) calculated the power density for different amplitudes ($St = 0.15 - 0.95$) in one-orifice baffles. The experimental results for low amplitudes ($St < 0.2$) where slightly higher than those predicted by the quasi-steady model (orifice coefficient $C_0 = 0.6$). However, the quasi-steady model underestimated the power density at lower oscillating amplitudes.

Baird and Stonestreet (1995) developed the eddy enhancement model, using the same experimental data measured by Mackley and Stonestreet (1995). This model tries to fix the quasi-steady model problem at high frequencies and low amplitudes. The model is based on the eddy turbulence coupled with the acoustic behaviour. The viscosity related to the vortices is modelled by introducing a new parameter: the mixing length l_m, corresponding to the average vortex travelled length. However, as the authors stated, the model must be calibrated for different tube diameters and fluid viscosities to select the appropriate value for the mixing length.

Table 1 collects the main characteristics of the two power density models available in the open literature.

Table 1
Available models for the calculation of the energy dissipation in OBRs.

Model	Quasi-steady (Mackley and Stonestreet, 1995)	Eddy-enhancement model (Baird and Stonestreet, 1995)
Power density	$\overline{\varepsilon}_v = \frac{2n_b\rho}{3\pi L_p C_0^2}\left(1/S^2 - 1\right)(2\pi f x_0)^3$	$\overline{\varepsilon}_v = 1.5\frac{\rho\omega^3 x_0^2 l_m}{l\cdot S}$
Characteristic parameter	Discharge coefficient, C_0	Mixing length, l_m
Reference values	$C_0 = 0.6$(Jealous and Johnson, 1955; Mackley and Stonestreet, 1995), $C_0 = 0.7$(Baird and Garstang, 1967)	$l_m = 7mm$(Baird and Stonestreet, 1995), $l_m = 9mm$(Baird and Rao, 1995)
Recommended range of application	x_0=5–30 mm, f=0.5–2 Hz	x_0=1–3 mm, f=5–14 Hz

CFD models for oscillatory flow reactors have been employed for analysing the existing models for energy dissipation, allowing for a broader range of operating conditions and baffle geometries. Jimeno et al. (2018) developed a CFD numerical model to validate the aforementioned models, applied to OBRs with smooth periodic constrictions (geometry NiTech© DN15). The authors studied two net Reynolds numbers (70 and 140) and a wide range of oscillatory Reynolds numbers (650–10000). The results showed that the quasi-steady model overestimates the power consumption. Based on these results, the authors proposed a quasi-steady model adapted to the geometry under study. The effect of the interaction between consecutive cells on the energy dissipation was modelled by using a power law dependency between the power density and the number of cells.

Avila et al. (2020) also studied the energy dissipation in an OBR with smooth periodic constrictions (geometry NiTech© DN15) using CFD. The study examines a range of low Reynolds numbers: $Re_n = 6 - 27$ and $Re_{osc} = 24 - 96$, showing that the quasi-steady model proposed by Jimeno et al. (2018) is not valid for OBRs operating in the laminar flow regime. The authors presented a new parameter, the dimensionless power density:

$$\left(\frac{\overline{W}_{osc}}{V}\right)^* = \frac{(\overline{W}_{osc}/V)D}{\rho(2\pi f x_0 + U_n)} \tag{3}$$

Thus, if the dimensionless power density is plotted against the oscillatory Reynolds number, it has a similar trend to the Power number used in stirred tanks: a decreasing linear relation in the laminar flow regime and a constant value in the chaotic flow regime.

Recently, Sutherland et al. (2020) studied the energy dissipation in OBCs with oscillating baffles using CFD. The authors introduced a Power number as a dimensionless quantity to characterise the energy dissipation in OBRs. However, the study does not check if the Power number only depends on the relevant dimensionless numbers and not on the fluid properties. A correlation for the Power number as a function of the oscillatory Reynolds number, Strouhal number and open cross sectional area is proposed for the range $Re_{osc} = 5000 - 20000$.

From the previous review, we can conclude that the two main models for energy dissipation in OBRs, quasi-steady and eddy enhancement models, show the same limitation: both require fitting parameters which highly vary depending on the operating conditions. However, there are no systematic studies focused on determining which values for the discharge coefficient or the mixing length are suitable for certain dimensionless flow conditions. The results are mainly provided in a dimensional form and, consequently, they are not valid for different fluids or scales. Furthermore, some dimensionless approaches have been introduced, (Hafez and Baird, 1978; Avila et al., 2020), but their impact is still scant because of the limited range tested and the lack of experimental results validating its suitability.

The main goal of this work is to demonstrate the applicability of a dimensionless number to account for the oscillatory power consumption using a purely experimental methodology. Other relevant aspects, seldom covered in the open literature, are studied in depth, as the role of the oscillatory pressure drop amplitude and the pressure drop-velocity phase-lag, which have an interest from a practical and physical point of view, respectively. For that purpose, a wide experimental campaign has been performed, measuring a large range of oscillatory Reynolds and Strouhal numbers, several working fluids and two different baffle geometries (with one and three orifices).

2. Methodology

2.1. Geometries under investigation

Two different baffle designs, with one and three circular orifices, are investigated in the present work. A sketch of these inserts with their relevant dimensions is shown in Fig. 1. Both baffles present the same open cross-sectional area, $S = 0.25$, following a widely used and recommended design criteria in the field of oscillatory baffled reactors (Ni et al., 1998). The distance between consecutive baffles is, however, dependent on the orifice diameter, $l = 3d$, to ensure a similar behaviour for different number of orifices (same length for expansion per orifice) (Smith, 1999). The baffle thickness is 1 mm in both cases.

2.2. Test rig

A hydraulic bench aimed at providing net and oscillatory flows along the test section is employed in order to characterize the oscillatory pressure drop in a wide range of operational conditions (see Fig. 2). The test section (5) consists of an AISI 316 stainless steel tube with 32 mm inner diameter, where the equally-spaced baffles are placed.

Two pressure taps machined in the tube wall connect the test section with the port holes of the piezoresistive sensors (9), which are used to measure the instantaneous oscillatory pressure drop. Four different fast response time pressure transducers have been used, two of them absolute (model KISTLER Type 4260A with range of 0–7 bara and 0–10 bara) and two differential (model KISTLER Type 4264A with range ±100 mbar and ±1 bar) to cover all the range of operating conditions tested.

With the aim of measuring the pressure drop where the flow has achieved spatially-periodic conditions and unaffected by entry effects, the first pressure tap is located at the middle position of the fifth cell for the MH1 geometry. The second pressure tap is located downstream, at a distance $L_p = 1296$ mm, corresponding to 27 cells for the geometry MH1. Again, five cells are located between
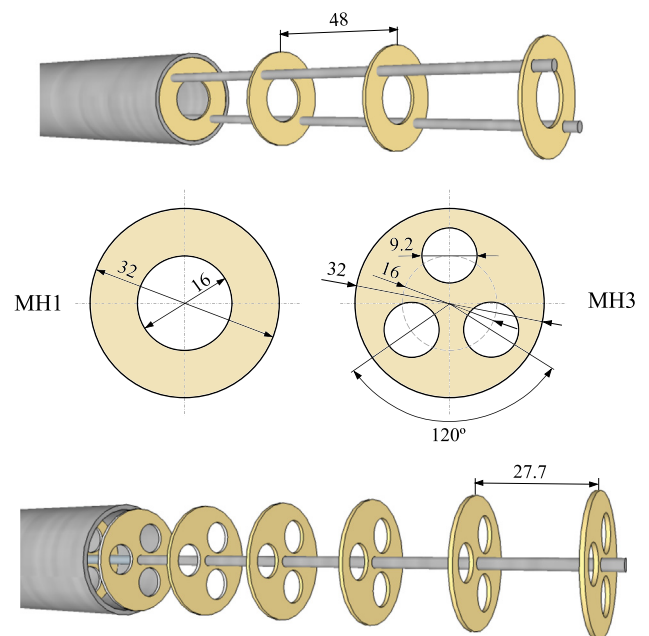

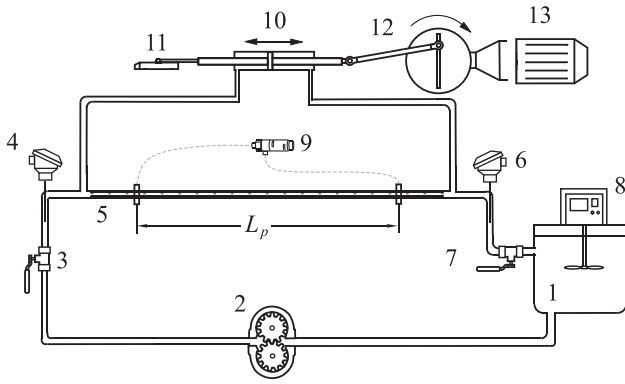**Fig. 1.** Geometries under investigation: MH1 and MH3 baffles (Dimensions in mm).

Fig. 2. Experimental set-up. (1) Reservoir tank, (2) gear pump, (3) manual valve, (4) PT-100 Class B 1/10 DIN temperature sensors, inlet, (5) baffles, (6) PT100 Class B 1/10 DIN, outlet, (7) manual valve, (8) mixer, (9) pressure transducers, (10) double acting cylinder, (11) displacement sensor, (12) crank and connecting rod, (13) gear reducer and motor.

the second pressure drop and the last baffle to avoid entry effects during flow reversal.

At both ends of the test section, the circuit is connected to the chambers of a reciprocating double-effect cylinder (10), creating the oscillatory loop. The movement of the cylinder is generated by an adjustable crank and rod arrangement (12), whose length ratio ensures a quasi-sinusoidal motion. The rotary motion is provided by a reducer-motor (13), which operates in a frequency range from 0.47 to 4.7 Hz. A magnetostrictive position sensor (11), model BALLUFF BTL6-A500-M0100, with a 2 kHz frequency measures the instantaneous position of the system.

The working fluid is pumped from the main reservoir (1) by a gear pump (2). A mixer (8) ensures that the fluid mixtures are homogeneous. To avoid cavitation, the oscillatory loop is properly pressurised at 4 barg by closing the outlet manual valve (7), and then the inlet manual valve (3) is closed to isolate the oscillatory loop from the rest of the circuit. The fluid temperature is obtained using the temperature measured at both ends of the test section with PT100 RTDs (4,6). All the test were performed under isothermal conditions at room temperature.

The fast response signals (position and pressure) have been acquired by a NI USB-6001 data acquisition card. The slow response measurements, temperature at both ends of the test section, are acquired by a datalogger, model 34980A.

In the search of validated non-dimensional results, the contribution of different thermo-physical properties to the results was analyzed using several mixtures propylene glycol–water, which have been tested at room temperature: 95 %, 80 % and 60 % propylene glycol for the geometry MH1; and 95 % and 60 % propylene glycol for the geometry MH3.

Fluid samples are taken from the test section periodically in order to measure the kinematic viscosity with a Cannon–Fenske viscometer. Using the measured viscosity at a known temperature, the mixture concentration can be inferred from water-propylene glycol mixtures tables, in order to retrieve other thermo-physical properties (ASHRAE, 2001).

2.3. Data reduction

To characterize the power consumption by means of the power density (Eq. (1)) or any other parameter, the average power, $\overline{W}_{osc}$, must be calculated from Eq. (4). The instantaneous pressure drop for the length between pressure ports, Δp_{AB}, and the instantaneous oscillatory velocity, u_{osc}, are used. Thus, no assumptions have been

made regarding the shape of the pressure drop and velocity waves (unlike Eq. (2)).

$$\overline{W}_{osc} = \frac{1}{T} \int_0^T A u_{osc} \Delta p_{AB}(t) dt \tag{4}$$

2.3.1. Filtering
In order to reduce the noise level of the raw signals, a smoothing algorithm has been applied. As an example, Fig. 3 displays the original and filtered pressure drop signals.

2.3.2. Oscillating amplitude
The amplitude of the fluid flow oscillation is obtained from the position signal measured by the magnetostrictive sensor. The center-to-peak amplitude can be derived from the maximun and minimum positions, however, in order to compensate the effect of the electrical noise, the local maximum and minimum are calculated for each cycle, and, finally, the mean value of the center-to-peak amplitudes for all the cycles is used.

It is taken into account that the cross sectional area of hydraulic cylinder and the tube of the test section are different. So, the real amplitude of the fluid movement in the test section is related to the amplitude of the cylinder oscillation assuming that the flow rate, in both cases, has to be the same, neglecting compressibility effects.

2.3.3. Oscillating frequency
The frequency with a higher amplitude is obtained after applying the Fast Fourier Transform to the position signal.

2.3.4. Instantaneous mean flow velocity
The instantaneous velocity is calculated from the instantaneous position data by using a numerical approximation of four points (Gautschi, 2012):

$$u(t) \approx \frac{1}{12\Delta t}(x_0(t + 2\Delta t) + 8x_0(t + \Delta t) - -8x_0(t - \Delta t) - x_0(t - 2\Delta t)) \tag{5}$$

The time step, Δt, must be chosen carefully since a low value may lead to a highly distorted velocity signal due to the noise level, while a high value can attenuate the real amplitude of the velocity signal.
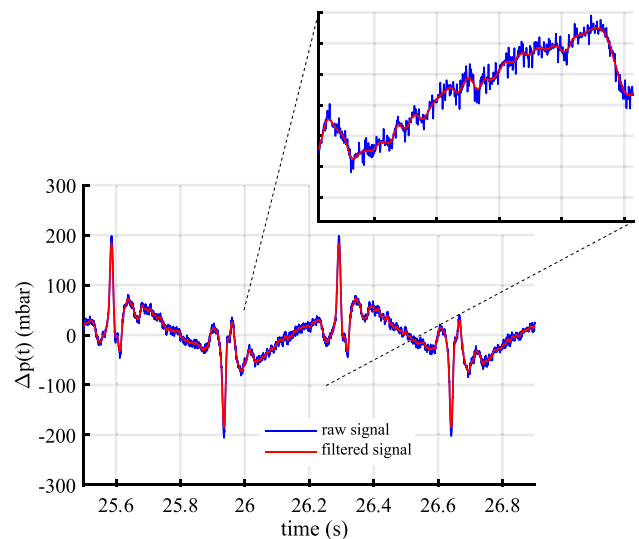

Fig. 3. Raw and filtered oscillating pressure drop signals.

2.4. Uncertainty analysis

An uncertainty analysis has been performed following the procedure described in Bejan and Kraus (2003), considering both the bias error (due to the sensors, using the data provided by the manufacturer) and the precision error (calculated from the standard deviation of the repeated measurements) for each variable. The uncertainty of the derived quantities is then obtained using the error propagation theory.

The estimated expanded uncertainty for the derived quantities of interest in this study are included in Table 2. The maximum and mean value for the uncertainty is included for the maximum and minimum amplitudes tested and for both baffle geometries. As can be seen, there are points with significant uncertainties (>20%) for both geometries at the lowest dimensionless amplitude tested. This uncertainty is mainly due to the low accuracy of the pressure sensors in comparison to the low amplitude of the pressure drop measured.

3. Pressure drop and power consumption results

In order to characterize the pressure drop, its amplitude and phase lag with the velocity signal must be calculated. Both variables have a significant effect on the power consumption calculation (Eq. (1)).

Theoretically, the phase lag can take any value from $\delta = 0$, when the pressure drop and velocity signals are in phase, corresponding to a purely frictional system and the power density is maximum; to $\pi/2$, which corresponds to a purely inertial system, where there is energy recovery during one half of the cycle and the power density would be zero.

3.1. Characterisation of the pressure drop and velocity signals

Eq. (2) is obtained assuming that the pressure drop is a perfect sine wave. However, this hypothesis is not fulfilled as has already been shown both numerically (Jimeno et al., 2018) and experimentally (Muñoz-Cámara et al., 2020), even when the instantaneous flow rate can be considered as sinusoidal. However, previous experimental and numerical studies (Baird and Stonestreet, 1995; González-Juárez et al., 2018) seem to omit this point, because the authors determined the amplitude as the maximum of the pressure drop signal and the phase lag from the zero crossings of the pressure drop and velocity signal. Thus, several assumptions, which are valid only when perfect sine waves are involved, have been used inappropriately.

Due to this problem, in this work we propose to determine the expressions of the sine waves which provide a better representation of the pressure drop and velocity signals to, afterwards, calculate their amplitudes and relative phase lag. Thus, simplicity is lost in order to avoid inconsistencies and use the simplified equation for the power density (Eq. (2)). Following this criterion, two methods have been used: (1) statistical fitting method and (2) Fast Fourier Transform method.

3.1.1. Statistical fitting method

This method is based on determining the parameters of the sine functions (amplitude, frequency and initial phase) which provide the best fitting, i.e., minimum mean squared error, to the original signals (pressure drop and velocity). Once the parameters are known, the phase lag can be obtained as the difference between consecutive peaks of the fitted signals. Regarding the pressure drop amplitude, Δp_{max}, it is directly obtained as a parameter of the statistical fitting.

It should be noticed that, because of the nonlinearity of the statistical fitting, the algorithm is sensitive to the initial estimation of the parameters (amplitude, frequency and initial phase) and, sometimes, the valid solution can not be found automatically. In order to mitigate these potential problems, the following procedure has been used:

- The data set (corresponding to a minimum of 20 cycles) is divided in a series of data packets, each one containing a total of 4–5 cycles. Each of these packets is statistically fitted to a sine function independently of the others.
- A set of measurements of amplitude and phase lag is obtained and, previously to the calculation of the mean value, the Chauvenet's criterion is applied in order to remove any outlier. In addition, the results which are not in the range with physical meaning, $0 \leqslant \delta \leqslant \pi/2$, are discarded.

This set of experimental measurements also provides a way to compute the uncertainty related to the repeatability of the measurements.

Fig. 4 shows the measured pressure drop and velocity waves for one test, and the corresponding statistical fitting for one of the
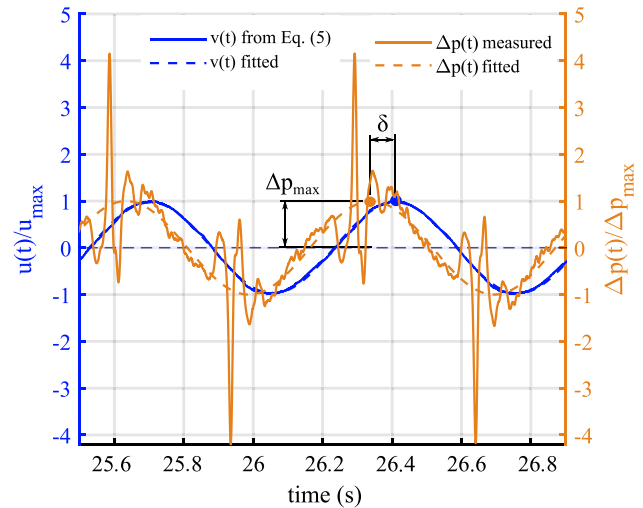

Fig. 4. Velocity and pressure drop signal, measured (continuous line -) and statistical fitting (dashed line –). MH1 Baffles, f = 1,41 Hz.

Table 2
Estimation of the uncertainty of the derived quantities.

Measurement	Average uncertainty (%)				Maximum uncertainty (%)			
-	MH1		MH3		MH1		MH3	
x_0/d	0.5	1.0	0.5	1.5	0.5	1.0	0.5	1.5
Dimensionless amplitude, x_0/D	3.2	1.6	5.2	1.9	3.2	1.6	5.4	2.0
Oscillatory Reynolds number, Re_{osc}	4.8	4.1	6.3	3.9	5.1	9.7	6.5	4.0
Pressure drop amplitude, Δp_{max}	9.0	3.8	7.1	2.2	42.9	19.1	24.4	7.6
Power density, $\overline{\varepsilon_v}$	9.2	4.7	9.8	3.2	38.0	19.2	25.1	7.9
Oscillatory Fanning friction factor, Re_{osc}	12.6	5.9	13.9	4.8	43.4	19.5	26.8	8.6
Phase lag, δ	0. 3	0.3	0.3	0.3	0.9	0.7	0.6	1.0
Power number,	12.3	5.8	13.5	4.7	42.1	19.2	25.7	8.5

packets of data. As can be observed, the velocity signal is close to a sine wave while the pressure drop is more complex, with a sharp fluctuation overlapping to a fundamental sinusoidal oscillation. The fluctuation reaches its peak when the velocity is close to zero, i.e., the end of the piston strokes. The fluctuation is due to the abrupt acceleration/deceleration when the piston reverses its movement. The peaks of both statistically fitted signals are highlighted in Fig. 4 to make the phase lag between both signals more evident.

3.1.2. Fast Fourier Transform method

This method is focused on obtaining the fundamental amplitude and frequency of both signals (pressure drop and velocity). Subsequently, the inverse Fast Fourier Transform is used to reconstruct the signal corresponding to the fundamental frequency and, finally, calculate the phase lag between those signals. Fig. 5 shows the measured pressure drop and velocity and the signals reconstructed using only their fundamental frequencies.

There is a clear phase lag, related to the inverse Fast Fourier Transform, between the measured and the reconstructed fundamental signal. However, this phase lag is the same for both the pressure drop and the velocity because the fundamental frequency is the same, thus, the relative phase δ between the reconstructed signals is the same as phase lag between the measured signals.

In Fig. 6, the amplitudes of the pressure drop (a) and the pressure drop-velocity phase lag (b) are plotted for the statistical fitting and Fast Fourier Transform methods. The results correspond to the measurements for the MH1 baffles at room temperature and with propylene glycol as working fluid.

Both algorithms provide very similar results for the phase lag, with a maximum relative deviation of around 1.5 % in the tested range, so they can be considered as equivalent in practice. Regarding the pressure drop amplitude, the results are also similar, but in this case the maximum relative deviation between both methods is as high as a 5 %. The values provided by the FFT method are systematically below those predicted by the statistical fitting, pointing out that there are still significant components in the frequency domain which are not considered by taking into account only the fundamental frequency. From this point forward, only the results obtained by the statistical fitting will be plotted. This decision is justified by two points: (1) it considers the whole real pressure drop signal to compute the 'equivalent' sine wave and (2) it is able to provide a good estimation of the measurements repeatability.
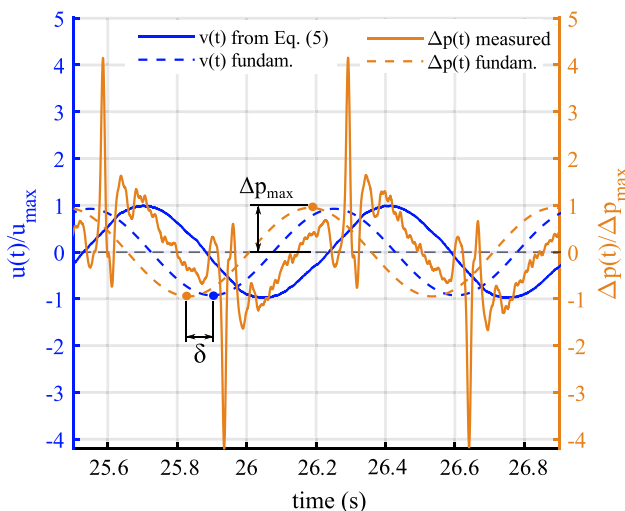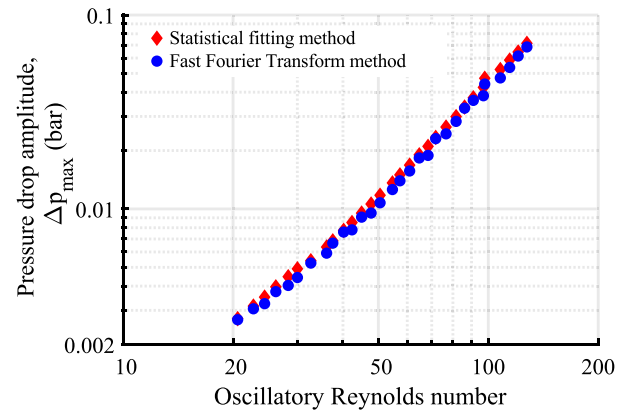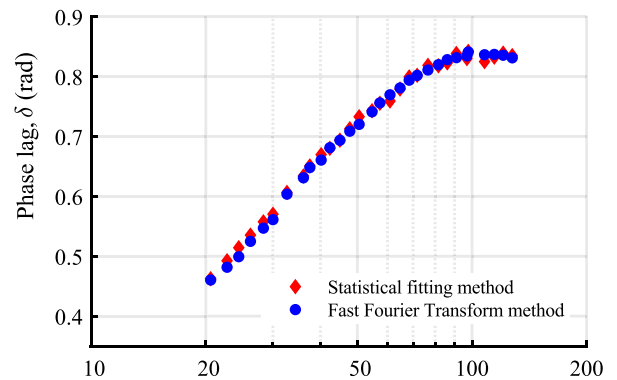

Fig. 5. Velocity and pressure drop signal, measured (continuous line -) and fundamental components from FFT (dashed line –). MH1 Baffles, $f = 1,41$ Hz.

(a)

(b)

Fig. 6. (a) Amplitude of the pressure drop and (b) pressure drop-velocity phase lag as a function of the oscillatory Reynolds number for both the statistical and Fast Fourier Transform algorithms.

3.2. Dimensional results

3.2.1. Pressure drop amplitude

The relation between the pressure drop amplitude and the maximum oscillatory velocity, $2\pi f x_0$, is represented in Fig. 7 for the MH1 baffles and two fluid mixtures. As can be seen, Fig. 7(a), the pressure drop amplitude, for a given maximum velocity, is significantly higher, around a 10%, for the most viscous fluid (95% propylene glycol). The amplitude follows a trend of $\Delta p_{max} \propto v_{max}^{2.1}$. This almost quadratic relation is remarkable because, in spite of the inertial component of the pressure drop, the trend is very close to that expected in a quasi-steady, purely frictional and turbulent internal flow.

In Fig. 7(b), the pressure drop amplitude shows a noticeable increase at lower oscillation amplitudes for the same maximum oscillatory velocity in all the range tested. For example, at a maximum velocity of 0.012 m/s there is an increase of more than 40% for a dimensionless amplitude $x_0/D = 0.25$ in comparison to the case with $x_0/D = 0.5$, an increment which is much higher than the uncertainty which corresponds to these measurements. It should be noticed that the oscillating frequency must be increased to keep the maximum oscillatory velocity at lower amplitudes.

3.2.2. Power density

The power density is plotted in Fig. 8(a) and (b) as a function of the maximum velocity for several working fluids and oscillating amplitudes, respectively. The power density (Fig. 8(a)) depends on the fluid properties, especially at low oscillatory velocities.
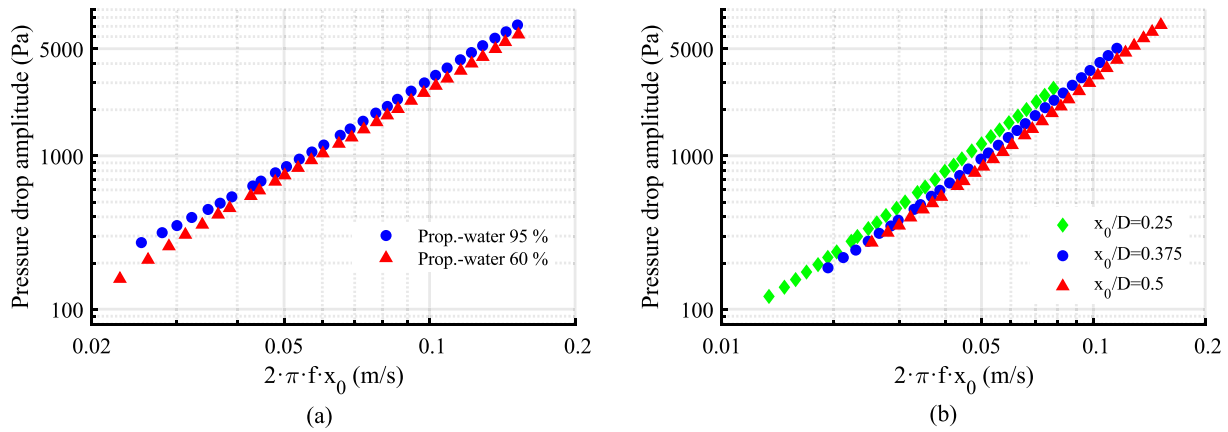
Fig. 7. Pressure drop amplitude as a function of the maximum oscillatory velocity for: (a) several working fluids and $x_0/D = 0.5$; (b) several amplitudes and 95% propylene glycol. MH1 baffles.
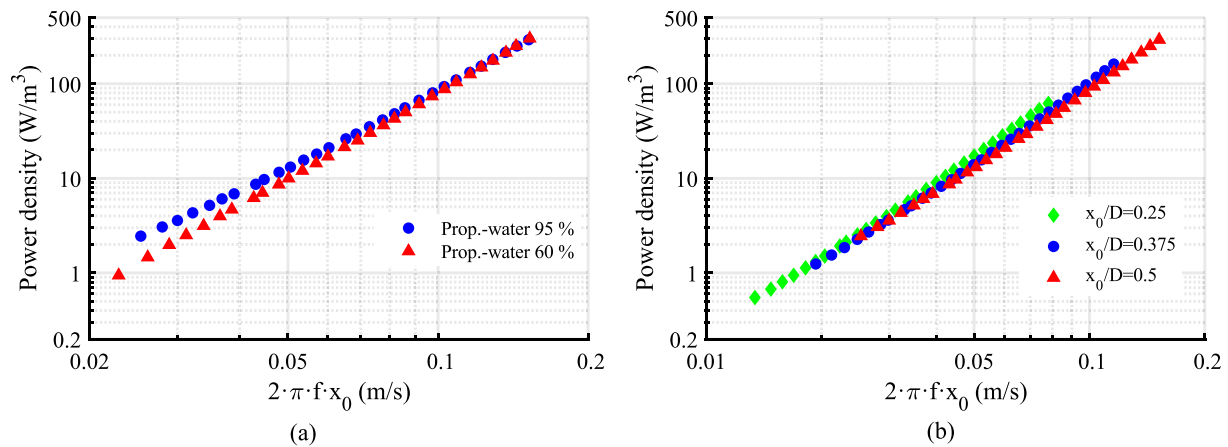

Fig. 8. Power density as a function of the maximum oscillatory velocity for: (a) different working fluids and $x_0/D = 0.5$; (b) different amplitudes and 95% propylene glycol. MH1 baffles.

According to the quasi-steady model, the trend should be a cubic function of the maximum velocity, however, the exponent (corresponding to the curve slope) is higher, around 3.5, at high oscillatory Reynolds numbers. As can be noticed, the slope for the fluid with higher viscosity (95% propylene glycol) is significantly lower at low velocities, which could indicate a change in the flow behavior.

Regarding the influence of the oscillating amplitude, in Fig. 8 (b) there is a slight but noticeable increase in the power density at lower dimensionless amplitudes and high maximum velocities. For example, for a maximum velocity of around 0.01 m/s there is an increase of a 25 % for the dimensionless amplitude $x_0/D = 0.25$ in comparison to the case with the highest dimensionless amplitude $x_0/D = 0.5$. The difference is, however, lower at low oscillatory velocities. It should be remarked that these differences are lower than those observed in the pressure drop amplitude, indicating that there should be a significant variation of the pressure drop-velocity phase lag, which is the remaining variable with an influence on the power density.

3.3. Review of previous models

The quasi-steady and eddy enhancement models are revisited in this section, by obtaining the model parameters (discharge coefficient and mixing length, respectively) that fit the measured data

set for the different oscillatory Reynolds numbers and dimensionless amplitudes tested.

3.3.1. Quasi-steady model

The power consumption predicted by the quasi-steady model is given by (Baird and Stonestreet, 1995):

$$\overline{W}_{qs} = \frac{n_b \rho (2\pi f x_0)^3 \left(1/S^2 - 1\right)}{1.5 C_0^2} \frac{D^2}{4} \tag{6}$$

Normally, previous studies have proposed a value for the discharge coefficient, C_0, that fits their results. However, the methodology is reversed here, the discharge coefficients obtained from the experimental measurements of power consumption. The discharge coefficient is plotted as a function of the oscillatory Reynolds number for the MH1 baffles in Fig. 9, for the three amplitudes and three working fluids that have been tested.

As can be observed, the definition of the discharge coefficient (Pritchard, 2011) is able to provide consistent dimensionless results (regardless of the fluid properties) for a given dimensionless amplitude. These values of the discharge coefficient can be introduced in Eq. (6) to predict the power density according to the quasi-steady model. The discharge coefficient varies significantly at low oscillatory Reynolds numbers, $Re_{osc} < 100$, in contrast to the constant values provided in the open literature, frequently in the range $C_0 = 0.6 - 0.8$ (Mackley and Stonestreet, 1995; Baird and
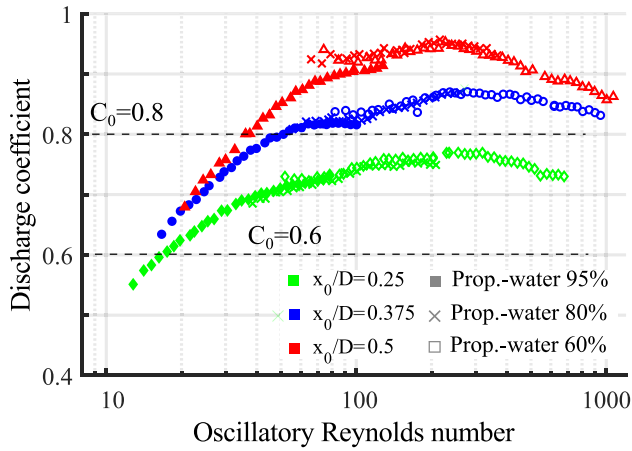
Fig. 9. Discharge coefficient as a function of the oscillatory Reynolds number for different oscillating amplitudes. MH1 baffles.

Fig. 10. Mixing length as a function of the oscillatory Reynolds number for several oscillating amplitudes. MH1 Baffles.

Rao, 1995). At higher oscillatory Reynolds numbers, $Re_{osc} > 100$, the discharge coefficient becomes more stable, justifying why it can provide good results for a given oscillating amplitude. The more stable discharge coefficient can be explained by the onset of the chaotic flow behaviour at $Re_{osc} > 150$ (Muñoz-Cámara et al., 2020).

It should be noticed that the orifice coefficient definition assumes: (1) an independent single orifice, while there are many baffles in series in OBRs, which are close enough to have flow interaction; (2) steady flow, while the flow is unsteady in OBRs. Thus, any conclusion based on the discharge coefficient should be carefully taken because it is a concept which oversimplifies the real physics of the problem.

In any case, the general trend of the discharge coefficient is similar to that observed in single orifices under steady flow conditions. For baffles with different open areas, Johansen (1930) observed the linear increase of the orifice coefficient at low Reynolds number (laminar flow), and a decrease (after a maximum value is reached) towards a lower and constant value at high Reynolds numbers.

These results show that the suitability of the quasi-steady model cannot be established based on dimensional quantities as frequencies and amplitudes, since it depends on the oscillatory Reynolds number and the dimensionless oscillating amplitude.

Another drawback related to the use of the discharge coefficient concept is that it can not be applied to more complex baffle geometries, as multiorifice baffles or helical baffles, without losing its physical meaning.

3.3.2. Eddy Enhancement model

The power consumption predicted by the eddy enhancement model (Baird and Stonestreet, 1995) is given by:

$$\overline{W}_{ee} = \frac{1.5 n_b \rho \omega^3 x_0^2 l_m}{S} \frac{\pi D^2}{4} \qquad (7)$$

Thus, with the measurement of the average energy dissipation (Eq. (4)) the corresponding mixing length can be calculated. In Fig. 10 the mixing length is plotted as a function of the oscillatory Reynolds number for the three different amplitudes and fluids tested for the MH1 baffles.

The mixing length also provides consistent results for each oscillating amplitude, however it should be considered that the problem of dimensionality could arise during scale-up, when the amplitude is changed in accordance to the OBR size to keep the same operating dimensionless numbers (Strouhal number or the equivalent dimensionless amplitude).
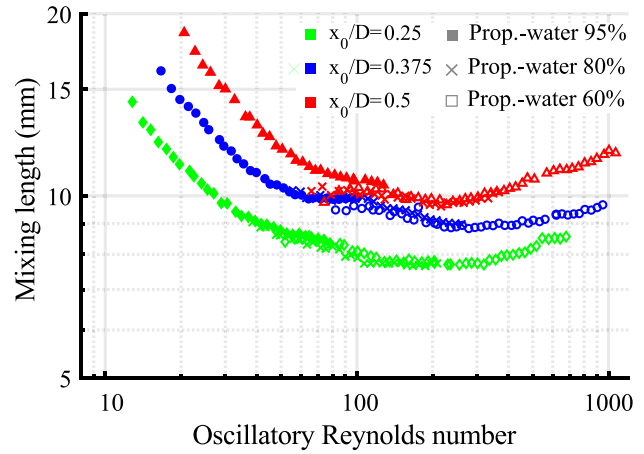
3.4. Dimensionless results

From the previous results, the complexity of the problem is evident: the flow behaviour seems to vary depending on the fluid properties and the oscillating amplitude. In the following section, we analyze the results in a more general dimensionless form.

3.4.1. Oscillatory Fanning friction factor

The pressure drop amplitude can be expressed in dimensionless form using the oscillatory Fanning friction factor, which is based on the definition of the friction factor used in pipes under steady flow. The fitted amplitude (see Section 3.1.1) of the pressure drop wave, Δp_{max}, and the maximum velocity of the oscillatory flow, $2\pi f x_0$, are taken as characteristic pressure drop and velocity, respectively.

$$f_{osc} = \frac{\Delta p_{max}}{2\rho(2\pi f x_0)^2} \frac{D}{L_p} \qquad (8)$$

This parameter has been widely used to characterize the pressure drop in oscillatory flows (Bagci et al., 2015; Costa et al., 2014; LLeong and Jineong and Jin, 2006).

3.4.2. MH1 baffles

In Fig. 11 the oscillatory Fanning friction factor is plotted as a function of the oscillatory Reynolds number for the three different amplitudes studied. For each amplitude, the results for the three mixtures are distinguished according to the their markers (solid, hollow or cross). As a reference, the net Fanning friction factor for the MH1 baffles under steady flow conditions (Muñoz-Cámara et al., 2020) is also plotted.

The most relevant result to be highlighted is the consistency of the results for different fluid properties. This confirms the adequacy of the oscillatory Fanning friction factor to characterize the oscillatory pressure drop amplitude.

At low oscillatory Reynolds numbers, the different curves are closer to the net Fanning friction factor results; it should be borne in mind that the behaviour at sufficiently low oscillatory Reynolds numbers should be quasi-steady and purely frictional, with the total instantaneous pressure drop equal to the pressure drop in a system with the same mean velocity under steady flow conditions. Under these circumstances, the maximum pressure drop and, consequently, the oscillatory Fanning friction factor would be identical to the net Fanning friction factor.

The trend for the three amplitudes is similar, decreasing at low oscillatory Reynolds numbers and more flattened at higher values. The first region would correspond to a laminar flow behaviour and the second one to a chaotic flow according to previous studies
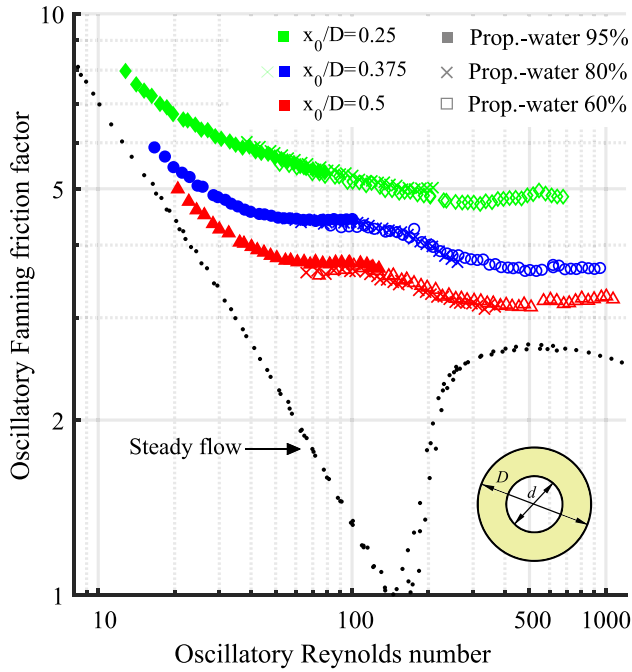
Fig. 11. Oscillatory Fanning friction factor vs oscillatory Reynolds number. MH1 baffles.

Fig. 12. Oscillatory Fanning friction factor vs oscillatory Reynolds number. MH3 baffles.

focused on flow visualization at an amplitude $x_0/D = 0.5$ (Mackay et al., 1991; Muñoz-Cámara et al., 2020; Zheng et al., 2007). The transition to a chaotic flow is much smoother for the oscillatory flow in comparison to the net flow case.

The friction factor increases with decreasing values of the oscillating amplitude (or increasing values of Strouhal number). For instance, at $Re_{osc} = 40$, a reduction in the dimensionless oscillating amplitude from $x_0/D = 0.5$ to $x_0/D = 0.25$ implies an increase in the Fanning friction factor of an order of 50 %. This effect has also been observed in previous experimental studies (Mackley and Stonestreet, 1995), where the authors showed that the pressure drop amplitude was higher at lower oscillating amplitudes and at the same maximum oscillatory velocity.

3.4.3. MH3 baffles

The results for the oscillatory Fanning friction factor are shown in Fig. 12 for the MH3 baffle design, at five different oscillating amplitudes. Since the nominal amplitude for the MH3 baffles is lower, $x_0 = d = 0.29D$, a wider range of dimensionless amplitudes has been reproduced in the test rig. Again, the Fanning friction factor for the net flow case is included as a reference (Muñoz-Cámara et al., 2020).

In this case, the trend of the oscillatory friction factor at low oscillatory Reynolds numbers is more evident, overlapping the net Fanning friction factor. This confirms that the flow behaviour is quasi-steady and purely frictional at low oscillatory Reynolds numbers.

A noticeable inconsistency can be observed for the different fluids at low amplitudes. This can be explained by the difference in oscillating amplitude, which had to be adjusted manually. The little deviation that has been measured, 0.2–0.4 mm, has a significant effect for low amplitudes (4–8 mm).

A similar trend can be observed for all the amplitudes tested, analogous to that obtained for the MH1 baffles.

3.4.4. Correlations

A modified Ergun's equation is considered (Eq. (9)). This equation provides a proper fitting to the smooth curvature of the mea-
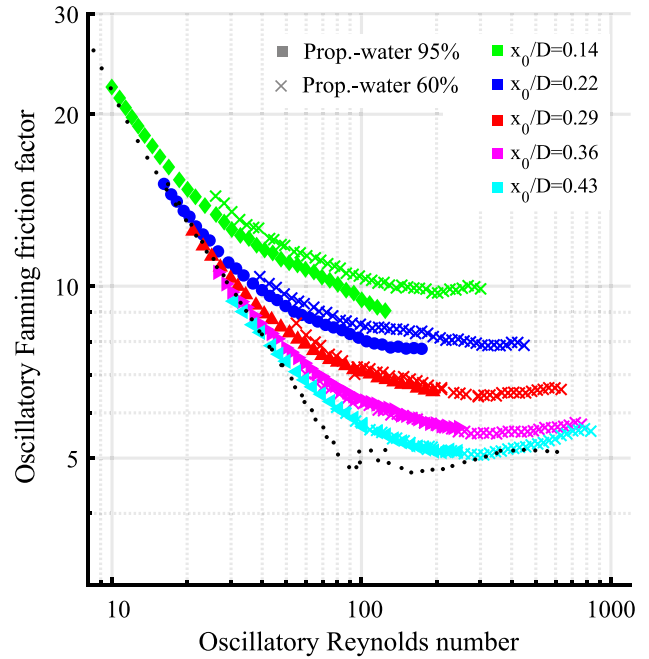
surements and has been used previously to fit data for the friction in oscillatory flows (Pamuk and Özdemir, 2012; Bagci and Dukhan, 2018).

$$f_{osc} = \frac{C_1}{Re_{osc}} + C_2 Re_{osc}^m \left(\frac{x_0}{D}\right)^n \tag{9}$$

The first term accounts for the decreasing trend at low oscillatory Reynolds numbers (corresponding to the laminar flow regime), where the effect of the dimensionless amplitude is negligible. The second term fits the curve behaviour at higher oscillatory Reynolds numbers (chaotic flow), where the amplitude effect is important and the trend, while more stable, has a slight slope.

In Table 3 the coefficients from the statistical fitting are provided for the two geometries tested. The maximum and mean relative deviation of the correlation from the experimental data is also given.

3.4.5. Pressure drop-velocity phase lag

The power density can be calculated in a simplified way, assuming that the velocity and pressure drop signals are perfectly sinusoidal, by Eq. (2), using the phase lag between them, δ. Thus, in spite of not being indispensable for the calculation of the energy dissipation, it is evident that the phase lag has a significant role in the energy dissipation. The phase lag also gives us the relative weight of the frictional and inertial components of the pressure drop, and it allows us to compare the trends observed with those provided in the open literature.

The pressure drop-velocity phased lag is quantified in radians, as a portion of the oscillating period, so it is a dimensionless parameter on its own.

3.4.5.1. MH1 baffles.
The phase lag is shown in Fig. 13 as a function of the oscillatory Reynolds number for the MH1 baffles. For the lower oscillatory Reynolds number tested, $Re_{osc} \approx 15$, the phase lag does not fall to zero, although there is a clear descending trend in the phase lag when the oscillatory Reynolds number is decreased. This supports the idea of the quasi-steady behavior

Table 3
Coefficients of the correlation for the oscillatory Fanning friction factor.

Baffles	C_1	C_2	m	n	$u_{max}(\%)$	$\bar{u}$ (%)
MH1	23.43	2.80	−0.0445	−0.586	7.3	2.1
MH3	152.5	1.76	0.0739	−0.666	7.2	1.9

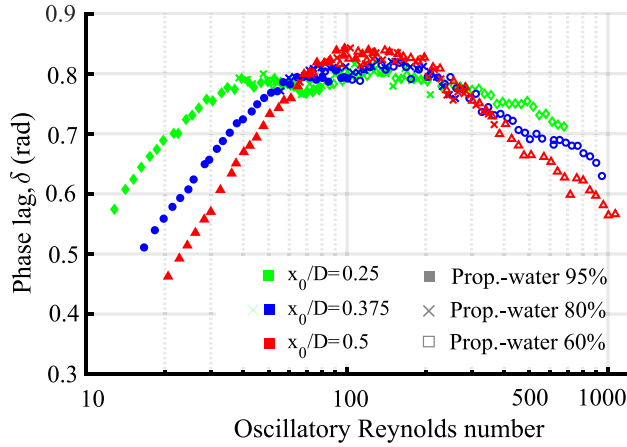**Fig. 13.** Pressure drop-velocity phase lag as a function of the oscillatory Reynolds number for several amplitudes and working fluids. MH1 baffles.

Fig. 14. Pressure drop-velocity phase lag as a function of the oscillatory Reynolds number for several amplitudes and working fluids. MH3 baffles.

which was previously presented with the oscillatory Fanning friction factor results in the low oscillatory Reynolds number region.

The decrease of the oscillating amplitude in this so-called unsteady laminar region has a substantial impact on the increase of the pressure drop-velocity phase lag. This phenomenon, which at constant Re_{osc} also implies an increase of the oscillating frequency, yields an increment on the effect of the fluid inertia on the pressure drop. At a higher oscillatory Reynolds number the phase lag tends to remain in a close range, around 0.8–0.85 radians, for all the amplitudes tested. Above $Re_{osc} \approx 200$, the trend is reversed, and the phase lag decreases up to 0.6 radians at the highest oscillatory Reynolds number tested. This trend suggests an increase in the frictional component of the pressure drop, which can be related to the onset of the chaotic flow regime (Muñoz-Cámara et al., 2020).

3.4.5.2. MH3 baffles. The results for the MH3 baffles (Fig. 14) follow a similar trend to the MH1 results. In both types of baffles, a lower oscillating amplitude leads to an increase in the phase lag. Consequently, because the nominal amplitude for the MH3 baffles is significantly lower, an increase in the phase lag should be expected. However, the phase lag for the MH3 baffles is lower than for the MH1 baffles. For instance, at $Re_{osc} = 50$ and $x_0/D = 0.5$ the MH1 baffles results show a phase lag $\delta = 0.84$ rad, while for the MH3 baffles is $\delta = 0.55$ rad for a lower amplitude, $x_0/D = 0.43$. Thus, it can be concluded that the MH3 baffles imply a significant rise of the frictional component of the pressure drop, which could be justified by the higher hydraulic diameter for the three orifice diameter baffles (70% higher) and/or the higher proximity to the tube walls of the jets generated by the orifices.

3.4.6. Power number

The evaluation of the energy dissipation in oscillatory flow reactors has been traditionally characterized by the power density, ε_v (Mackley and Stonestreet, 1995). However, the main problem of this parameter is that is not dimensionless. In order to solve this aspect, the Power number is proposed in this work in order to
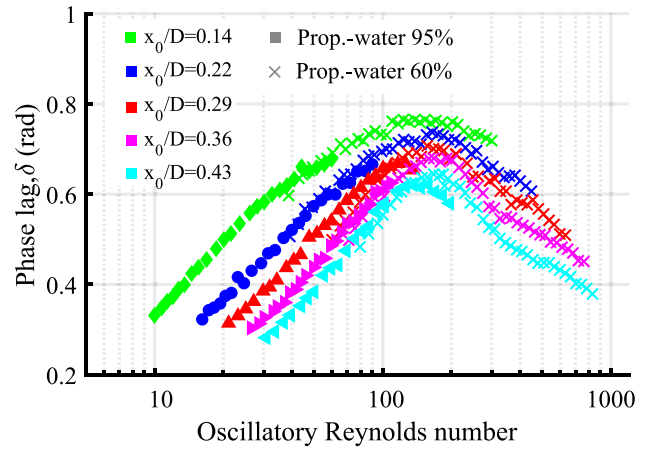
characterise the energy dissipation. This dimensionless number, widely used in stirred tanks (Couper et al., 2005), is defined as:

$$Po = \frac{\overline{W}_{osc}}{\rho N^3 D^5} \tag{10}$$

where N is the stirring velocity. In OBRs, the characteristic angular velocity can be taken as: $2\pi f$, and the characteristic length as the cell tank length, l. Thus, the Power number definition applied to OBRs is:

$$Po = \frac{\overline{W}_{osc}}{n_b \rho (2\pi f)^3 D^5} \tag{11}$$

This definition was already used by González-Juárez (2017), showing that it can provide consistent dimensionless results. However, it should be noticed that the power consumption provided by the quasi-steady model (Eq. (6)) is proportional to the cube of the maximum velocity, $(2\pi f x_0)$, and, consequently, the Power number can be reformulated as suggested by Sutherland et al. (2020):

$$Po = \frac{\overline{W}_{osc}}{n_b \rho (2\pi f x_0)^3 D^2} \tag{12}$$

This way, for a given geometry (diameter D, open area fraction S and discharge coefficient C_0), the definition of the Power number is equivalent to comparing the real power consumption to the value predicted by the quasi-steady model. This definition would also be similar to the parameters presented by Hafez and Baird (1978) or Avila et al. (2020).

The definition of the Power number is now obtained as a function of measured variables: pressure drop amplitude, Δp_{max}, and pressure drop-velocity phase lag, δ:

$$Po = \frac{1}{32\pi} \frac{\Delta p_{max} \cos \delta}{n_b \rho (f x_0)^2} \tag{13}$$

The only assumption made is that both pressure and velocity signals can be fitted to sine waves and, consequently, can be characterized by their amplitudes and phase lag.

3.4.6.1. Relation with previous models. From the definition of the Power number, for n_b baffles, the power consumption can be expressed as:

$$\overline{W}_{osc} = n_b \rho (2\pi f x_0)^3 D^2 Po \tag{14}$$

Matching Eqs. 14 and 6 we can find a relation between the orifice coefficient and the Power number:

$$C_0^2 = \frac{1/S^2 - 1}{6Po} \tag{15}$$

Thus, the discharge coefficient is related to the Power number directly for analogous geometries, i.e., same open area fraction, S, and number of orifices, n_o.

Matching Eqs. 14 and 7 we can find a relation between the mixing length and the Power number:

$$l_m = \frac{8S}{3\pi} x_0 Po \tag{16}$$

The mixing length is related to the Power number for a given geometry and amplitude. The problem is that the mixing length is proportional to the oscillating amplitude, so it should not be expected that a given mixing length could be used for similar OBRs with different amplitudes.

3.4.6.2. MH1 baffles. Experimental results of the Power number as a function of the oscillatory Reynolds number are represented in Fig. 15. As expected, the results are appropriately dimensionless for the different fluids. The trend is similar for the three amplitudes: a decreasing slope at low oscillatory Reynolds numbers, while at higher values there is a minimum and a slightly positive slope, which is related to the decrement of the pressure drop-velocity phase lag at higher oscillatory Reynolds numbers. This general trend is similar to that observed in stirring tanks (Couper et al., 2005): a decreasing trend at low Reynolds numbers corresponding to a laminar flow behaviour and a region approximately constant where the flow is considered as turbulent.

Another aspect to be highlighted is that the three curves for different oscillating amplitudes overlap at low oscillatory Reynolds numbers. This effect was also observed for the oscillatory Fanning friction factor, but is more noticeable in the Power number results. This makes sense because in a quasi-steady flow the power consumption should not change with the oscillating amplitude but with the maximum oscillatory velocity and, consequently, with the oscillatory Reynolds number.

As a reference, numerical results from Avila et al. (2020) and Jimeno et al. (2018) are also plotted. Only data with the following conditions are considered: (1) similar conditions to a pure oscillatory flow, i.e., low net Reynolds number in comparison to the oscillatory Reynolds number, and (2), similar cell length-diameter ratio and open area fraction to our study. The main difference is the baffle geometry, both studies are focused on an OBR with smooth constrictions.
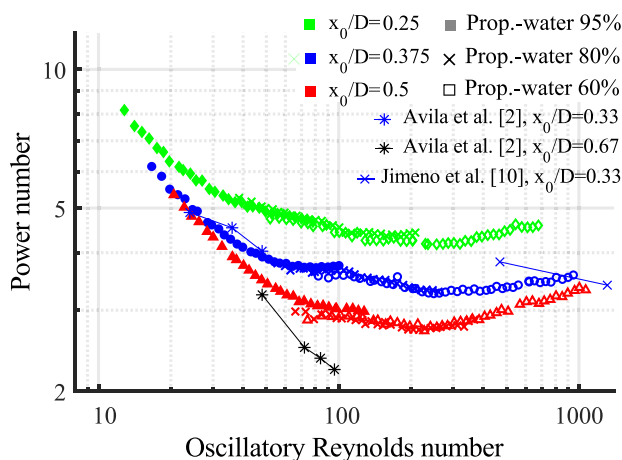
As can be seen, the data for $x_0/D = 0.33$ are close to those obtained in this study for $x_0/D = 0.375$, and the trends are similar: a decreasing slope in the laminar region and more stable values in the chaotic flow region. It is true that lower values could be expected due to the smooth constrictions in comparison to the baffles here tested. However, it should be taken into account that the numerical results include the effect of the net flow while this study has no net flow.

The results from Avila et al. (2020) at $x_0/D = 0.67$ are far below the experimental results at $x_0/D = 0.5$, but, at low oscillatory Reynolds number, the trend seems to follow the same as the laminar region tests. In addition, the numerical results are coherent with the general trend observed in this study: a higher dimensionless oscillating amplitude leads to a lower Power number.

3.4.6.3. MH3 baffles. The results for the MH3 baffles (Fig. 16) show a trend very similar to that observed for the MH1 baffles, with all the curves for different amplitudes overlapping at low oscillatory Reynolds numbers. It is more evident for this geometry that the change in the slope of the curve is delayed, i.e., at lower amplitudes the deviation takes place at a lower oscillatory Reynolds number at which the flow changes its behaviour. This could be related to a sooner onset of the chaotic flow at lower oscillating amplitudes, however the lack of experimental visualization results in this range does not allow us to confirm this point.

3.4.6.4. Correlations. In order to provide correlations to make easier the application of the results, a modified Ergun's equation for all the amplitudes tested is considered again (Eq. (17)).

$$Po = \frac{C_1}{Re_{osc}} + C_2 Re_{osc}^m \left(\frac{x_0}{D}\right)^n \tag{17}$$

In Table 4 the coefficients from the statistical fitting are provided for the two geometries tested. The maximum and mean relative deviation of the correlation from the experimental data is also given.
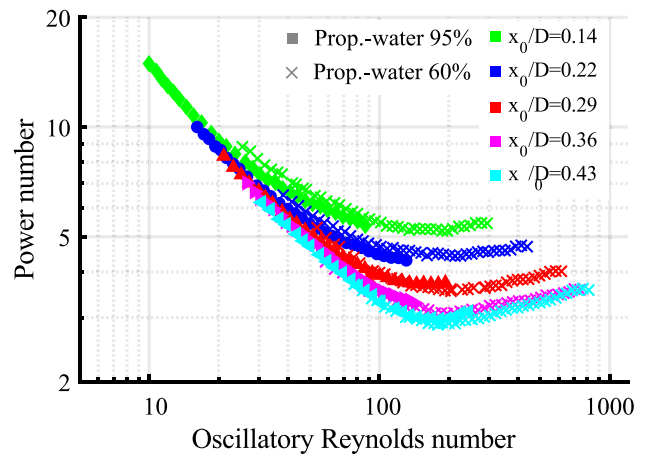

Fig. 16. Power number as a function of the oscillatory Reynolds number for several amplitudes and working fluids. MH3 baffles.

Table 4
Coefficients of the correlation for the Power number.

Baffles	C_1	C_2	m	n	u_{max}(%)	$\bar{u}$ (%)
MH1	61.85	1.01	0.0906	−0.680	11.8	2.4
MH3	130.2	0.53	0.189	−0.622	9.8	3.1

Fig. 15. Power number as a function of the oscillatory Reynolds number for several amplitudes and working fluids. MH1 baffles.

4. Conclusions

Time-resolved pressure drop measurements of oscillatory flow in a baffled tube have been performed in a hydraulic test rig under isothermal conditions. One-orifice and three-orifice baffles have been tested. Instantaneous measurement of the piston displacement has allowed to derive the oscillatory velocity signal. The maximum oscillatory pressure drop and the maximum oscillatory velocity, as well as the phase lag between signals, are obtained from their statistic fitting and the FFT analysis. The subsequent data reduction and analysis of results has allowed us to derive the following outcomes:

- For both types of baffles and low oscillatory Reynolds numbers, an increase in the oscillatory Reynolds number leads to an augmentation of the pressure drop-velocity phase lag up to a maximum value. Beyond this critical oscillatory Reynolds number, $Re_{osc} \approx 150$, there is a decreasing trend in the phase-lag, suggesting a transition to chaotic flow. This critical value is similar to the value at which previous studies found the onset of an asymmetric flow.
- Oscillatory Fanning friction factor is a consistent dimensionless number to evaluate the maximum pressure drop as a function of oscillatory Reynolds number and dimensionless oscillating amplitudes. For very low values of Re_{osc}, of the order of 10, the flow behaviour is almost quasi-steady and purely frictional.
- The Power number has been applied, for the first time, to experimental pressure drop measurements in OBRs, obtaining proper dimensionless results for different working fluids.
- Power number becomes independent of the oscillating amplitude at low values of Re_{osc}, as a result of the quasi-steady nature of the flow in this regime.
- For a given oscillatory Reynolds number, a reduction of the dimensionless amplitude (or an increasing of the Strouhal number) leads to an increase of the oscillatory Fanning friction factor, the pressure drop-velocity phase-lag and the Power number.
- Smooth curvature of the oscillatory Fanning friction factor and the Power number curves has allowed to fit the data using a modified Ergun's equation, with a maximum deviation of $\approx 10\%$.

Declaration of Competing Interest

The authors declare that they have no known competing financial interests or personal relationships that could have appeared to influence the work reported in this paper.

Acknowledgments

References

ASHRAE, 2001. ASHRAE fundamentals handbook.

Avila, M., Fletcher, D.F., Poux, M., Xuereb, C., Aubin, J., 2020. Predicting power consumption in continuous oscillatory baffled reactors. Chem. Eng. Sci. 212, 115310.

Bagci, O., Dukhan, N., 2018. Impact of pore density on oscillating liquid flow in metal foam. Exp. Thermal Fluid Sci. 97, 246–253.

Bagci, Ö., Dukhan, N., Özdemir, M., 2015. Characteristics of oscillating liquid flow in foam-like highly-porous media: An experimental study. Exp. Thermal Fluid Sci. 60, 96–105.

Baird, M.H.I., Garstang, J.H., 1967. Power consumption and gas hold-up in a pulsed column. Chem. Eng. Sci. 22, 1663–1673.

Baird, M.H.I., Rao, N.R., 1995. Power dissipation and flow patterns in reciprocating baffle-plate columns. Canad. J. Chem. Eng. 73, 417–425.

Baird, M.H.I., Stonestreet, P., 1995. Energy dissipation in oscillatory flow within a baffled tube. Chem. Eng. Res. Des. 73, 503–511.

Bejan, A., Kraus, A.D., 2003. Heat transfer handbook.

Costa, S.C., Tutar, M., Barreno, I., Esnaola, J.A., Barrutia, H., García, D., González, M.A., Prieto, J.I., 2014. Experimental and numerical flow investigation of Stirling engine regenerator. Energy 72, 800–812. https://doi.org/10.1016/j.energy.2014.06.002.

Couper, J., Penney, W., Fair, J., Walas, S., 2005. Chemical Process Equipment.

Daily, J.W., Hankey Jr, W.L., Olive, R.W., Jordaan Jr, J.M., 1955. Resistance coefficients for accelerated and decelerated flows through smooth tubes and orifices. MASSACHUSETTS INST OF TECH CAMBRIDGE 55-SA-78.

Eze, V.C., Harvey, A.P., 2018. Continuous reactive coupling of glycerol and acetone – A strategy for triglyceride transesterification and in-situ valorisation of glycerol. Chem. Eng. J. 347, 41–51. https://doi.org/10.1016/j.cej.2018.04.078.

Gautschi, W., 2012. Numerical Analysis. Second ed.

González-Juárez, D., 2017. Comportamiento termofluidodinámico y transporte de especies en reactores de flujo oscilatorio con deflectores multiperforados.

González-Juárez, D., Herrero-Martín, R., Solano, J.P., 2018. Enhanced heat transfer and power dissipation in oscillatory-flow tubes with circular-orifice baffles: a numerical study. Appl. Therm. Eng. 141, 494–502. https://doi.org/10.1016/j.applthermaleng.2018.05.115.

Graca, C.A., Lima, R.B., Pereira, M.F.R., Silva, A.M., Ferreira, A., 2020. Intensification of the ozone-water mass transfer in an oscillatory flow reactor with innovative design of periodic constrictions: Optimization and application in ozonation water treatment. Chem. Eng. J. 389, 124412. https://doi.org/10.1016/j.cej.2020.124412.

Hafez, M.M., Baird, M.H.I., 1978. Power consumption in a reciprocating plate extraction column. Trans IChemE 56, 229–238.

Jealous, A.C., Johnson, H.F., 1955. Power requirements for pulse generation in pulse columns. Industr. Eng. Chem. 47, 1159–1166. https://doi.org/10.1021/ie50546a021.

Jimeno, G., Chu, Y., Ni, X.w., 2018. On the evaluation of power density models for oscillatory baffled reactors using CFD. Chem. Eng. Process.: Process Intensif. 134, 153–162. https://doi.org/10.1016/j.cep.2018.11.002.

Johansen, F., 1930. Flow through pipe orifices at low Reynolds numbers. Proc. Royal Soc. 126, 231–245.

Leong, K.C., Jin, L.W., 2006. Characteristics of oscillating flow through a channel filled with open-cell metal foam. Int. J. Heat Fluid Flow 27, 144–153. https://doi.org/10.1016/j.ijheatfluidflow.2005.05.004.

Liu, Y.C., Dunn, D., Lipari, M., Barton, A., Firth, P., Speed, J., Wood, D., Nagy, Z.K., 2019. A comparative study of continuous operation between a dynamic baffle crystallizer and a stirred tank crystallizer. Chem. Eng. J. 367, 278–294.

Mackay, M., Mackley, M., Y., W., 1991. Oscillatory flow within tubes containing wall or central baffles. Trans IChemE 69, 506–513.

Mackley, M.R., Stonestreet, P., 1995. Heat transfer and associated energy dissipation for oscillatory flow in baffled tubes. Chem. Eng. 50, 2211–2224.

McDonough, J.R., Phan, A.N., Harvey, A.P., 2015. Rapid process development using oscillatory baffled mesoreactors - A state-of-the-art review. Chem. Eng. J. 265, 110–121. https://doi.org/10.1016/j.cej.2014.10.113.

Muñoz-Cámara, J., Crespí-Llorens, D., Solano, J., Vicente, P., 2020. Experimental analysis of flow pattern and heat transfer in circular-orifice baffled tubes. Int. J. Heat Mass Transf. 147, 118914. https://doi.org/10.1016/j.ijheatmasstransfer.2019.118914.

Muñoz-Cámara, J., Crespí-Llorens, D., Solano, J.P., Vicente, P., 2020. Baffled tubes with superimposed oscillatory flow: experimental study of the fluid mixing and heat transfer at low net Reynolds numbers. Exp. Thermal Fluid Sci. 110324.

Muñoz-Cámara, J., Solano, J., Pérez-García, J., 2020. Experimental correlations for oscillatory-flow friction and heat transfer in circular tubes with tri-orifice baffles. Int. J. Therm. Sci. 156, 106480. https://doi.org/10.1016/j.ijthermalsci.2020.106480.

Ni, X., Brogan, G., Struthers, A., Bennett, D.C., Wilson, S.F., 1998. A systematic study of the effect of geometrical parameters on mixing time in oscillatory baffled columns. Chem. Eng. Res. Des. 76, 635–642. https://doi.org/10.1205/026387698525162.

Onyemelukwe, I.I., Nagy, Z.K., Rielly, C.D., 2020. Solid-liquid axial dispersion performance of a mesoscale continuous oscillatory flow crystalliser with smooth periodic constrictions using a non- invasive dual backlit imaging technique. Chem. Eng. J. 382, 122862. https://doi.org/10.1016/j.cej.2019.122862.

Pamuk, M.T., Özdemir, M., 2012. Friction factor, permeability and inertial coefficient of oscillating flow through porous media of packed balls. Exp. Therm. Fluid 38, 134–139. https://doi.org/10.1016/j.expthermflusci.2011.12.002.

Pritchard, P., 2011. Introduction to fluid mechanics. .

Smith, K.B., 1999. The Scale-Up of Oscillatory Flow Mixing. https://core.ac.uk/download/pdf/1334175.pdf.

Sutherland, K., Pakzad, L., Fatehi, P., 2020. Oscillatory power number, power density model, and effect of restriction size for a moving-baffle oscillatory baffled column using CFD modelling. Canad. J. Chem. 98, 1172–1190. https://doi.org/10.1002/cjce.23713.

Zheng, M., Li, J., Mackley, M.R., Tao, J., 2007. The development of asymmetry for oscillatory flow within a tube containing sharp edge periodic baffles. Phys. Fluids 19, 1–15. https://doi.org/10.1063/1.2799553.